Title	Silica-coated Mn-doped ZnS nanocrystals for cancer theranostics
Author(s)	Edison Huixiang Ang, Jialiu Zeng, Gomathy Sandhya Subramanian, Vijila Chellappan, Thankiah Sudhaharan, Parasuraman Padmanabhan, Balázs Gulyás, and Subramanian Tamil Selvan
Source	*ACS Applied Nano Materials, 3*(3), 3088–3096
Published by	American Chemical Society

Silica-Coated Mn-Doped ZnS Nanocrystals for Cancer Theranostics

Edison Huixiang Ang,[1,2,†*] Jialiu Zeng,[1,3,‡] Gomathy Sandhya Subramanian,[1] Vijila Chellappan,[1] Thankiah Sudhaharan,[4,5,§] Parasuraman Padmanabhan,[6] Balázs Gulyás,[6] and Subramanian Tamil Selvan [1,6,‖,*]

[1] A*STAR Institute of Materials Research & Engineering, 2 Fusionopolis Way, Innovis, Singapore 138634

[2] National Institution of Education, Nanyang Technological University, 1 Nanyang Walk, Singapore 637616

[3] Department of Biomedical Engineering, Boston University, Boston, MA 02215, USA

[4] Institute of Medical Biology, A*STAR, Singapore 138648

[5] Skin Research Institute of Singapore, A*STAR, Singapore 138648

[6] Translational Neuroscience Laboratory, Lee Kong Chian School of Medicine, Nanyang Technological University, 59 Nanyang Drive, Singapore 636921

[†] Present address: National Institution of Education, Nanyang Technological University, 1 Nanyang Walk, Singapore 637616

[‡]Present address: Department of Biomedical Engineering, Boston University, Boston, MA 02215, USA

[§]Present address: Skin Research Institute of Singapore, A*STAR, Singapore 138648

[‖]Present address: Translational Neuroscience Laboratory, Lee Kong Chian School of Medicine, Nanyang Technological University, 59 Nanyang Drive, Singapore 636921

ABSTRACT: Doped nanocrystals such as manganese – doped zinc sulfide (ZnS:Mn) are useful nanomedicine probes for cancer cell labelling and anticancer drug delivery. However, the synthesis and retention of fluorescence of these nanocrystals is highly indispensable for efficient cell theranostics. Herein, we report a modified synthesis of highly fluorescent hydrophobic ZnS:Mn nanocrystals with the advent of dual-ligands. Our results demonstrate that the alkylamine ligand with the carbon chain length of C_{18} promotes the diffusion of Mn from surface into interior of ZnS nanocrystals. Optical measurements show that the quantum yield of Mn (QY_{Mn}) can reach as high as 80% in the presence of a dual ligand combination of oleylamine–octadecylamine, due to the increased probability of $^4T_1 \rightarrow {}^6A_1$ emission, originating from the energy transfer of ligated nanocrystals. These doped nanocrystals after ligand

exchange of organic ligands with glutathione exhibited a high retention of quantum yield (QY: ~50-60%), and further coating with silica showed the QY of ~35-40%. Finally, we show the application of these doped nanocrystals for cancer theranostics such as HeLa cell labeling, and anti-cancer drug delivery.

KEYWORDS: *Doped nanocrystals, zinc sulfide, Mn dopant, ligand chemistry, cancer nanotheranostics*

1. INTRODUCTION

Nanoparticles and nanostructures based on metals, oxides and polymers have been widely studied for theranostics of cancer[1-3] and neurodegenerative disorders.[4-7] On the other hand, semiconductor nanocrystals or quantum dots (e.g. CdSe/ZnS) have been well exploited for biological applications over the last decade.[8-10] However, the toxicity due to carcinogenic Cd has been a major concern, which warrants the development of visible emitting Cd-free quantum dots for biological applications. Previously, aqueous dispersions of blue emitting ZnO quantum dots with a high photoluminescence quantum yield (PL-QY) were reported.[11] Conversely, NIR based Ag_2S QDs are superior to visible emitting nanocrystals owing to their potential for in vivo bioimaging.[12-14]

The aim of our current work was to synthesize highly fluorescent-doped nanocrystals as a counterpart to the most studied CdSe/ZnS QDs. Doped nanocrystals are preferred over visible emitting CdSe and NIR emitting PbS QDs, because the latter QDs involve heavy carcinogenic metals.

In recent years, doped semiconductor nanocrystals owing to their optical and magnetic properties, are attracting significant attention in diverse fields such as spintronic[15-16] and biological applications.[17-20] The underlying mechanism that controls doping is the adsorption of impurities (dopants) on the surface of nanocrystal, which is determined by surface morphology, nanocrystal size/shape and ligands in the growth solution.[21-22] In particular, manganese (Mn) has been studied widely as an impurity because of its multifunctional optical and magnetic properties.[23-24]

Over the years, several research groups have used different experimental strategies to gain better control and understanding of the doping mechanisms. Pradhan and co-workers have investigated the nucleation-doping strategy and found that the decoupling of doping from nucleation and growth is a key to the achievement of highly luminescent doped nanocrystals.[25-31]

Although most of the work in the literature focused on the nanocrystal growth time, temperature, Mn dopant concentration and Zn to S molar ratio of the precursors,[32-35] less efforts devoted to the effects of ligands on Mn-doping. Hence it is extremely important to discern the contribution of a particular ligand to the doping effect and to obtain quantitative information on the kinetics of dopant adsorption process, which is crucial for establishing a trapped-dopant model.[36] This model suggested that the binding energy of ligand relative to the host or dopant is an important factor for impurities incorporation.

Until now, the highest PL-QY of Mn (QY_{Mn}) in as-synthesized doped semiconductor nanocrystals (e.g. ZnSe, CdS/ZnS) reported is around 50%.[25-31, 37] Here we report a dual ligand approach to the synthesis of doped nanocrystals and provide a mechanistic study based on ligand base strength and orbital

interactions of dopant-ligand complex for obtaining highly fluorescent ZnS:Mn nanocrystals with a QY_{Mn} of ~80% for the first time.

Doped nanocrystals with a high QY in water or biological buffer are highly desirable for biological applications.[18, 38-40] It is worth mentioning here some of the common surface functionalization methods that exist in the literature for the preparation of water-soluble nanoparticles, nanoclusters and quantum dots. Among these, silica coating has been considered as one of the well-developed methods for quantum dots and nanoparticles.[41-49] Other most common coating methods involve either polymer,[50-52] peptides,[10, 53] lipids/liposomes,[54-55] or proteins[56, 57] for the stabilization of nanoparticles.

In this report, we have demonstrated the retention of a higher QY_{Mn} in water or biological buffers (up to 60%) upon ligand exchange with a short chain peptide, glutathione (GSH). Later, we have incorporated these ZnS:Mn@GSH nanocrystals into mesoporous silica, resulting in ZnS:Mn@GSH@silica nanocrystals with a QY_{Mn} of up to 40%. Finally, we have shown the applications of these doped nanocrystals for the labelling of cancer cells and drug delivery.

2. EXPERIMENTAL SECTION

Materials. Zinc chloride ($ZnCl_2$, 98%), Manganese(II) chloride tetrahydrate ($MnCl_2.4H_2O$, 98%), Sulfur powder (S, 99.999%), 1-octadecene (ODE, 90%), oleylamine (OAm, 70%), dodecanethiol (DDT, 98%), oleic acid (OAc, 99%), stearic acid (SA, 95%), octadecanethiol (ODT, 98%), octadecylamine (ODA, 97%), Rhodamine 6G (dye content 99%), 2-aminopyridine (99%), sulphuric acid (H_2SO_4, 95-98%), chloroform ($CHCl_3$, 99%) and methanol (MeOH, 99.8%), glutathione and tetraethyl orthosilicate were purchased from Sigma-Aldrich.

Synthesis of Highly Fluorescent Hydrophobic ZnS:Mn Doped Nanocrystals. In most of the syntheses, the primary ligand (L_1) used was OAm. Other secondary ligands (L_2) used were DDT, OAc, SA, ODT, ODA or OAm. First, $ZnCl_2$ (0.4 mmol) and $MnCl_2.4H_2O$ (0.08 mmol) were dissolved in 10 mL of DI H_2O. An equivalent volume of 800 µL (0.5 M of $ZnCl_2$**)** and 800 µL (0.1 M of $MnCl_2.4H_2O$) was transferred into a 100 mL three neck round bottom flask and heated to 120 ^oC to evaporate water. After cooling down to room temperature, S (0.4 mmol), 5 mL of OAm and 3 mmol of a secondary ligand was added to the reaction vessel for each experiment. The mixture was heated up to 250 ^oC and held for 20 min under Argon atmosphere.

Synthesis of Mn-doped ZnS with ODE as solvent and other secondary ligands (L_2): Similar procedures used as described above, except that the solvent OAm replaced by ODE.

Synthesis of Mn-doped ZnS with OAm and varying molar concentration of ODA: Similar procedures used as described above except that the concentration of ODA varied at 3, 6 and 12 mmol for three different samples.

Synthesis of Mn-doped ZnS with one (OAm or ODA) or two excess alkylamines (OAm+ODA): An 800 µL of 0.5 M of $ZnCl_2$ and 800 µL of 0.1 M of $MnCl_2.4H_2O$ added into 100 mL three neck round bottom flask and heated up to 120 ^oC, and later cooled down to room temperature. In order to see the effects of individual ligand on Mn-doped ZnS nanocrystal, three experiments were further designed as in the following: (i) To the cooled mixture, S (0.4 mmol), and OAm (18 mmol) added; (ii) cooled mixture, S (0.4 mmol), ODA (18 mmol); (iii) cooled mixture, S (0.4 mmol), OAm:ODA (15 mmol : 3 mmol). Finally, the mixture heated at 250^oC for 20 min under argon atmosphere.

Purification of Nanocrystals. All hydrophobic nanocrystals were purified three times with chloroform/methanol (1:3 volume ratio) and centrifuged at 3500 rpm for 10 min, and finally stored in 5 mL of chloroform for further analysis.

Water-soluble Nanocrystals. Glutathione (GSH)-coated doped nanocrystals (ZnS:Mn@GSH) were synthesized as follows: An aqueous GSH solution (300 µL; 120 mg/mL) added to the ZnS:Mn nanocrystals solution (1 ml of 1 mg/mL), and then 100 µL TMAH (tetramethyl ammonium hydroxide in 2-propanol/methanol mixture) added to deprotonate the carboxyl and thiol groups. The mixture was stirred overnight and the aqueous layer containing the ZnS:Mn@GSH particles was carefully separated and purified by adding ~ 2 mL of ethanol and centrifuged at 6000 rpm for 5 min. The recovered fluorescent pellet dispersed in cyclohexane and ethanol (1:1 volume ratio) was centrifuged twice and finally dispersed in water.

ZnS:Mn@GSH@Silica nanocrystals were prepared as in the following: GSH-coated doped nanocrystal (ZnS:Mn@GSH; 500 µL) was added to a solution containing 100 µL of 20 % tetraethyl orthosilicate (TEOS), cetyltrimethyl ammonium bromide (CTAB; 7.5 mL of 0.8 mM), and 200 µL of 0.1 M NaOH, and stirred for 2 days. Finally, ZnS:Mn@GSH@Silica nanocrystals were purified by routine centrifugation and re-dispersion cycles, and dispersed in water or buffer.

Materials Characterization. Transmission electron microscopy (TEM) and high-resolution (HR)-TEM analyses were performed with JEOL TEM 2100. The UV-visible absorption spectra were recorded using UV3600 Shimadzu UV-Vis-NIR spectrophotometer and photoluminescence (PL) spectra were acquired with a Shimadzu RF-5301PC fluorescence spectrophotometer. Inductively Coupled Plasma-Optical Emission Spectrometry (ICP-OES) analysis was acquired with the Dual-view Optima 5300 DV ICP-OES

system. The Fourier Transform Infrared Spectroscopy (FTIR) (Perkin Elmer Spectrum 2000) was used to obtain the spectra for nanocrystal solution dropped onto the KBr pellets. Powder X-ray diffraction (XRD) measurements were acquired with Bruker GADDS instrument.

Determination of Photoluminescene Quantum Yield. Mn-doped ZnS nanocrystals were excited at 325 nm and their emissions were observed at 405 nm and 585 nm. 2-aminopyridine and Rhodamine 6G dye were used as reference standards for bandgap (BG) blue emission at 405 nm and dopant Mn orange emission at 585 nm, respectively. Optical densities of the nanocrystal solution and dyes were kept below 0.12 at 325 nm. The quantum yield ratio, QY_{Mn}/QY_{BG} was extracted from the above optical spectra where QY_{Mn} is the quantum yield of Mn and QY_{BG} is the quantum yield of bandgap emission. This ratio represents the amount of Mn per nanocrystal.[33, 37]

Life-Time Measurements. Time resolved emission measurements were performed using Edinburg Laser Flash photolysis spectrometer (LP920-KS) in multiple emission map configuration. The samples were excited with a flash lamp pumped Q-switched Nd: YAG laser operating in a third harmonic wavelength of 355 nm (Ekspla NT 341A) and the emission spectra were acquired with an i-CCD (Andor) controlled by the computer. The emission spectra for different time delays after the laser excitation were measured. The average emission lifetimes were estimated by slicing and converting the spectral data into kinetic plot.

Cell Culture and Cytotoxicity Assays. All cell culture materials and reagents were procured from Invitrogen, Singapore. We followed our protocol reported earlier.[38] Briefly, both HeLa (human cervix adenocarcinoma) and CHO-K1 (Chinese Hamster Ovary) cells were grown in Dulbecco's modified Eagle's medium (DMEM) supplemented with 10% fetal bovine serum, 100 units/mL penicillin, and 100 µg/mL streptomycin and cultured in a 5% CO_2 humidified atmosphere at 37°C. For cell cytotoxicity, 10^4 cells per well were seeded in a 96-well plate. Following the incubation overnight, the cell culture medium was removed and 100 µL of either ZnS:Mn@GSH or ZnS:Mn@GSH@Silica nanocrystals diluted in phenol-free DMEM were added to the cells. The cells treated with the above nanocrystals were used for assessing the metabolic activity of cells using 3-(4,5-dimethylthiazol-2-yl)-2,5-diphenyltetrazolium bromide (MTT) colorimetric assays. A Tecan Infinite 200 microplate reader was used for the measurement of absorbance at 450 nm.

The percentage of cell viability[38] was calculated for cells treated with ZnS:Mn@GSH and ZnS:Mn@GSH@Silica samples at different concentrations by using the following equation:

$(A_t - A_b/A_c - A_b) \times 100$

Where A_t is the absorbance of the test compound (nanocrystals), A_b is the absorbance of the blank (culture medium and MTT solution), and A_c is the absorbance of the control (culture medium with cells and MTT solution).

Cell labelling. The HeLA cells were grown in 6-well plates (cell density of 1x 10^5 cells) with sterilized cover slips for 24 h with the respective media as described earlier. Nanocrystal samples of ZnS:Mn@GSH@Silica (100-150 µL of 0.1 $mgmL^{-1}$ stock solution) were added to each well containing cells and incubated for 2 h. After incubation, the cover slips were thoroughly washed with PBS and the cells were fixed by adding 4% paraformaldehyde. Finally, the cover slips were mounted on slides with one drop of Hydromount (National Diagnostics, USA). Olympus-Live Cell Inverted microscopy (IX81; CoolSNAP HQ camera and metal halide lamp; Metamorph software; 40x lens) was used with DAPI, Wheel QD580 and Wheel RFP filters. The images were exposed for different exposure times starting from the lowest until the best image was seen. The estimated exposure time of 10 ms (DIC), 2000 ms (Wheels RFP and QD580) were used for both nanocrystal-treated and control cells to rule out the autofluorescence. Finally, the image analysis was performed using the FUJI version 2.8 software.

3. RESULTS AND DISCUSSION

Design of Ligands and Characterization of Nanocrystals. The synthesis protocol for hydrophobic and water-soluble nanocrystals is shown schematically in Figure 1. Briefly, a mixture of $ZnCl_2$, $MnCl_2.4H_2O$, sulfur (S), oleylamine and octadecylamine (OAm+ODA) was heated at 250 ^oC under argon atmosphere to initiate the nucleation and growth of Mn-doped ZnS nanocrystals (denoted as ZnS:Mn). Glutathione (GSH), a short chain peptide was used to obtain water-soluble ZnS:Mn@GSH nanocrystals by a facile ligand exchange method. In order to further improve the photostability and prepare as a carrier for drug loading, mesoporous silica coating was employed to obtain ZnS:Mn@GSH@Silica. These water-soluble nanocrystals were finally explored for biological applications. Purification of nanocrystals is highly essential for biological applications, which is generally accomplished through centrifugation and dialysis. The hydrodynamic diameter and zeta potential of ZnS:Mn@GSH nanocrystals were estimated to be around 94.75 nm and -38.6 mV, respectively. However, the hydrodynamic size of ZnS:Mn@GSH@Silica nanocrystals were relatively larger (>200 nm) with the zeta potential values ranging from -10.5 mV to +25 mV. We further noted that our centrifuge-purified (but non-dialysed) silica-coated samples showed a large particle size distribution with the hydrodynamic diameter of 500 nm – 1 µm. The fluorescent digital images of nanocrystals are shown in the Supporting Information (Figure S1).

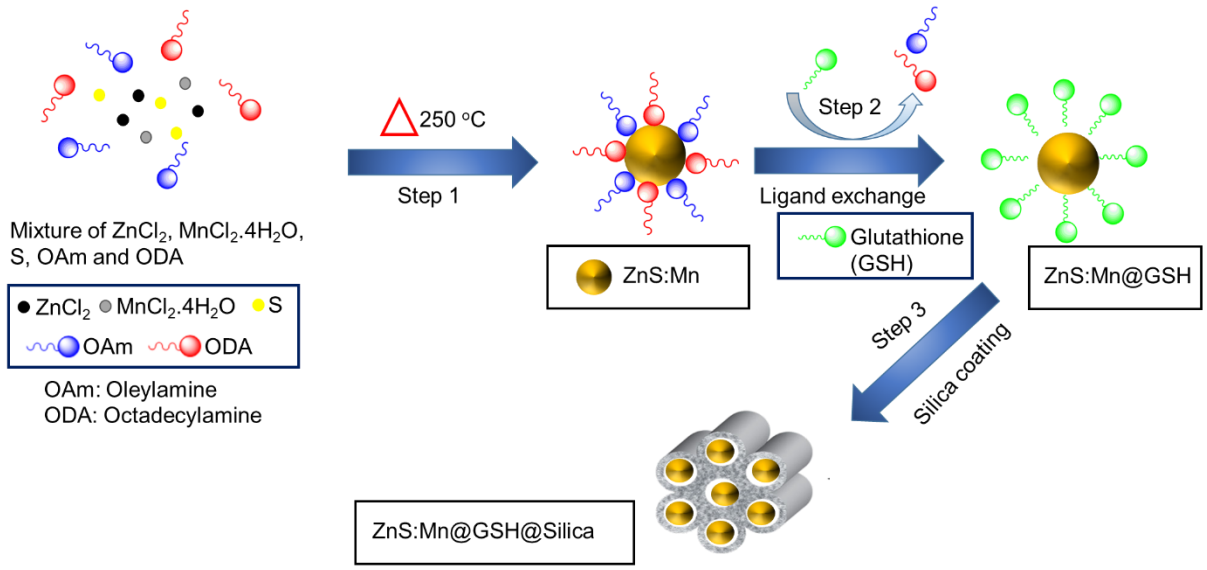

Figure 1. A schematic representation for the synthesis of highly fluorescent Mn-doped ZnS nanocrystals using dual ligands, oleylamine and octadecylamine (Step 1); water-soluble nanocrystals through glutathione ligand exchange (Step 2), and silica-coated nanocrystals (Step 3). See experimental section for detailed synthesis.

First, we delineate the role of ligands in dictating highly fluorescent hydrophobic ZnS:Mn nanocrystals. Figures 2A and 2B depict the schematic representation of different combinations and structures of ligands, respectively, used in this study. Representative high-resolution transmission electron microscopy (HRTEM) and scanning TEM (STEM) images of ZnS:Mn nanocrystals are shown in Figures 2C and 2D. The nanocrystals synthesized from a dual ligand combination of oleylamine and octadecanethiol (OAm+ODT), are quasi-spherical in shape with a mean diameter of *ca*. 5 nm (Figure 2C). The STEM image (Figure 2D) of nanocrystals synthesized from another dual ligand combination – oleylamine and octadecylamine (OAm+ODA) shows that the mean particle size is around 3.4 nm.

Here oleylamine (OAm) is the primary ligand (denoted as L_1). The size of doped nanocrystals with different ligand combinations (L_1: OAm and secondary ligand, L_2: DDT, OAc, SA, ODT, ODA) ranged from *ca*. 3.5-6 nm (Figures S2 and Figure S3). Although most of the doping methods in literature resulted in zinc-blende nanocrystal, our X-ray diffraction patterns exhibited wurtzite structure (Figure 2E and Figure S4) in consonance with previous reports on wurtzite-type alloy $Zn_xCd_{1-x}S$ nanocrystal[58] and wurtzite Mn-doped ZnS nanorod.[24]

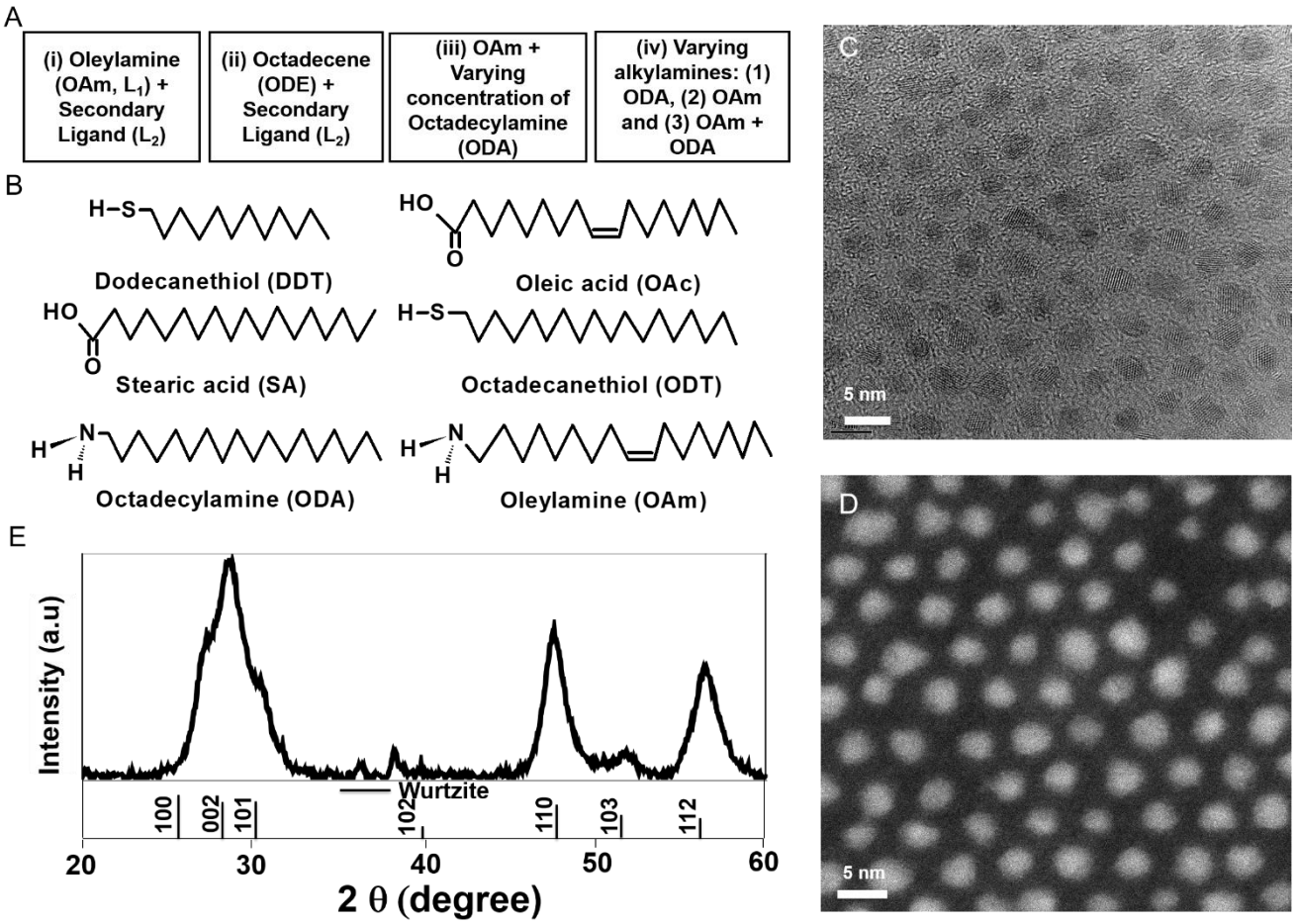

Figure 2. (A) Different combinations of ligands and solvents (oleylamine, OAm or octadecene, ODE) and (B) Structures of ligands. (C) Typical transmission electron microscopy (TEM) image of doped ZnS:Mn nanocrystals with dual ligands, oleylamine and octadecanethiol (OAm+ODT). (D) Scanning TEM (STEM) image of doped nanocrystals with oleylamine and octadecylamine (OAm+ODA). (E) X-ray diffraction (XRD) pattern of doped nanocrystals with the dual ligand combination of (OAm+ODA).

Optical Properties of Nanocrystals. In order to see the concentration effect of ODA on the optical properties of doped nanocrystals, a fixed volume of 5 mL OAm as dopant-growth solution was used, but with a variation in the concentration of ODA from 3, 6 to 12 mmol in the synthesis. The absorption spectra (Figure 3A) are identical with a broad band at around 310 nm for all the three concentrations. However, the PL spectra (Figure 3B) are different, exhibiting the blue emission bandgap quantum yield (QY_{BG}) of ZnS (1-23%) and orange emission quantum yield of Mn, QY_{Mn} (17-79%). At the initial concentration of 3 mmol ODA, the QY_{Mn} was 52%. When more ODA was added into the reaction, the QY_{BG} of ZnS (23%) was found to be quenched to 1% and the QY_{Mn} reached an optimum value of 79% at the moderate concentration of 6 mmol, followed by a decrease in QY_{Mn} (17%) at the highest concentration, 12 mmol.

It is obvious that the increase in ODA concentration (6 mmol) increased the binding strength of Mn to ZnS nanocrystal surface and incorporation of more surface Mn^{2+} ions into the lattice host, thereby contributing to an enhanced QY_{Mn} of 79%. However, an excess of Mn^{2+} ions substituted into the ZnS host might have caused the Mn-Mn spin interaction,[59] and therefore decreased the QY_{Mn} to 17% at the highest concentration of 12 mmol ODA.

Time-resolved PL measurements (Figure S5) and life-time decay plots (Figures 3C, 3D) showed that Mn-doped nanocrystals with ODA exhibited a very fast decay of ZnS blue emission in a shorter time domain (on the order of nanoseconds) compared to the orange emission (on the scale of milliseconds).[32] We have found that (OAm+ODA) functionalized nanocrystals with a higher QY showed the lifetimes of 19 ns and 0.31 ms for ZnS blue and Mn orange emissions, respectively. Nevertheless, (OAm+ODT) functionalized nanocrystals with a lower QY exhibited those corresponding lifetimes of 55 ns and 0.67 ms. This implies that some of the excited defect states in the low QY sample de-excites without blue emission, most probably via a nonradiative energy transfer to the Mn states. In consonance with earlier reports,[23, 32] the increase in overlap between the host and dopant wave functions in a nanocrystal may lead to an enhancement in the QY and a reduction of the radiative lifetime of the Mn orange emission, due to an enhanced energy transfer between the host and dopant levels.

There are several factors governing the optical properties (emission and QY_{Mn}) of doped nanocrystals. First, we have to consider the Mn geometry, which plays an important role.[35, 59] Earlier studies confirmed that the nanocrystal with tetrahedral Mn (T_d-Mn) geometry produced $^4T_1 \rightarrow {}^6A_1$ orange emission. On the other hand, doped nanocrystal with octahedral Mn (O_h-Mn) geometry failed to generate this orange emission. Importantly, the orange emission and QY_{Mn} are dictated by the tetrahedral Mn (T_d-Mn) geometry resulting from the substitution of Mn into tetrahedral Zn sites inside the lattice host of ZnS nanocrystals.[25] Next, we considered other two important factors: (i) bulkiness of the ligand and (ii) basicity of the ligand. These two factors can affect not only the geometry of Mn formed but also the binding strength of Mn to the nanocrystals.

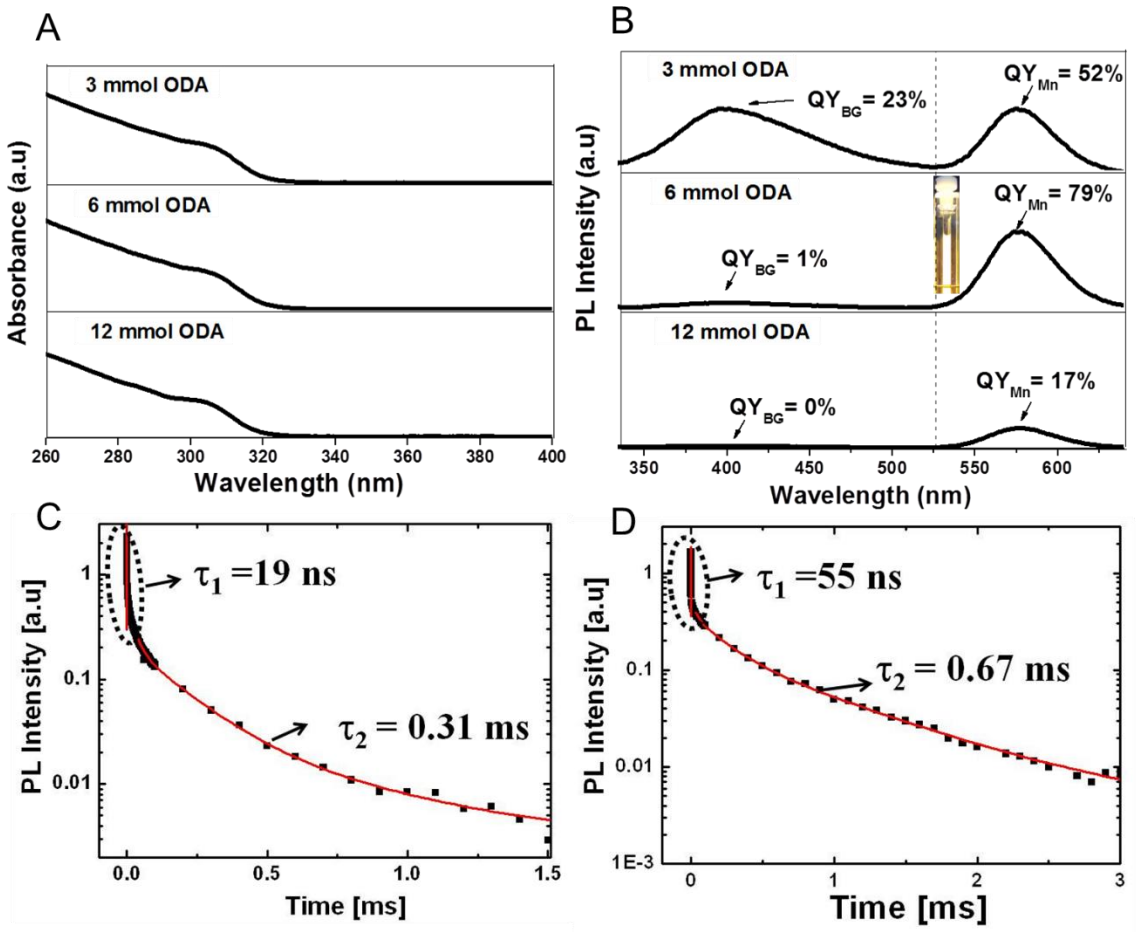

Figure 3. (A) Absorption and (B) photoluminescence (PL) spectra of ZnS:Mn nanocrystals functionalized with different molar concentration of ODA (3, 6 and 12 mmol) in 5 mL OAm. The quantum yields of band gap blue emission (QY_{BG}) and Mn orange emission (QY_{Mn}) are also given. (C, D) Life-time decay plots (Y-axis in logarithmic scale) of ZnS:Mn nanocrystals functionalized with (C) [OAm+ODA] and (D) [OAm+ODT] dual ligands. The average lifetime of ZnS and Mn emissions for [OAm+ODA] and [OAm+ODT] –functionalized nanocrystals are 19 ns and 0.31 ms, and 55 ns and 0.67 ms, respectively.

Geometry of Metal-Ligand Complex. Both steric and electronic effects of metals and ligands dictate the geometry. The steric effect is caused by the size of the metal and bulkiness of the ligand, while the electronic effect is associated with the electronic configuration of the metal and the base strength of the ligand. We neglected the electronic configuration and the size of Mn^{2+} ions as they are consistent in all different samples studied. Next, we considered other two important factors: (i) bulkiness of the ligand and (ii) base strength of the ligand. These two factors can affect not only the geometry of Mn formed but also the binding strength of Mn to the nanocrystals.

Figure 4A exhibits the FTIR spectra with two Mn-S bands at 1010 and 670 cm^{-1} and one Zn-S band at 615 cm^{-1} for nanocrystals functionalized with (ODE+ODA) and (OAm+ODA). Interestingly, the

nanocrystals functionalized with (OAm+ODA) showed an additional Zn-S band at 1110 cm^{-1}. Since ODA is a good sigma (σ) donor, it can coordinate strongly to the Mn center. Based on the molecular orbital theory, we assume that our ligated nanocrystals have uniform size and shape in order to possess the symmetry elements such as symmetry axis (principal axis, C_n) and plane of symmetry (vertical, σ_v).

The number of solvent molecules adsorbed or bound to Mn and ligand moecules coordinated to Mn is schematically shown in Figure 4B. As illustrated in Figure 4B (path- i), the plane of symmetry causes the weakening of the Mn-S band at 1010 cm^{-1} and disappearance of Zn-S band at 1110 cm^{-1} for nanocrystals functionalized with ODA in ODE (Figure 4A- i, and Figures S6, S7). This suggests that the ligand (ODA) in solvent (ODE) underperforms, resulting in weakly bound Mn. When the solvent was changed from ODE to OAm, the scenario is different, as depicted in Figure 4B (path ii), where the symmetry of plane is absent. This sample contained two ligands, OAm (L_1) and ODA (L_2), which are good σ donors with a different basicity, resulting in different π back donation strength in d_{xz} and d_{yz} orientations (Figure 4C). As a result, a distinct Zn-S band at 1110 cm^{-1} was observed for (OAm+ODA) – functionalized nanocrystals (Figure 4A).

Furthermore, (OAm+ODA) -functionalized nanocrystals showed a higher amount of Mn (ca. 2.5) per nanocrystal than that of Mn (ca. 0.2) for the control sample (ODE+ODA), as represented by the QY_{Mn}/QY_{BG} ratio (Figure 4D). These results indicate that in the presence of dual ligands (OAm+ODA), Mn is strongly bound to the nanocrystals, as illustrated in Figure 4B (path ii), resulting in a higher QY_{Mn} of 52% (Figure 4D). Furthermore, not all functionalized nanocrystals with (ODE+L2) showed orange emission, but other functionalized nanocrystals with (OAm+L_2) showed orange emission at 302 nm excitation. This indicates that (OAm) is a key solvent in promoting the incorporation of Mn into ZnS nanocrystals.

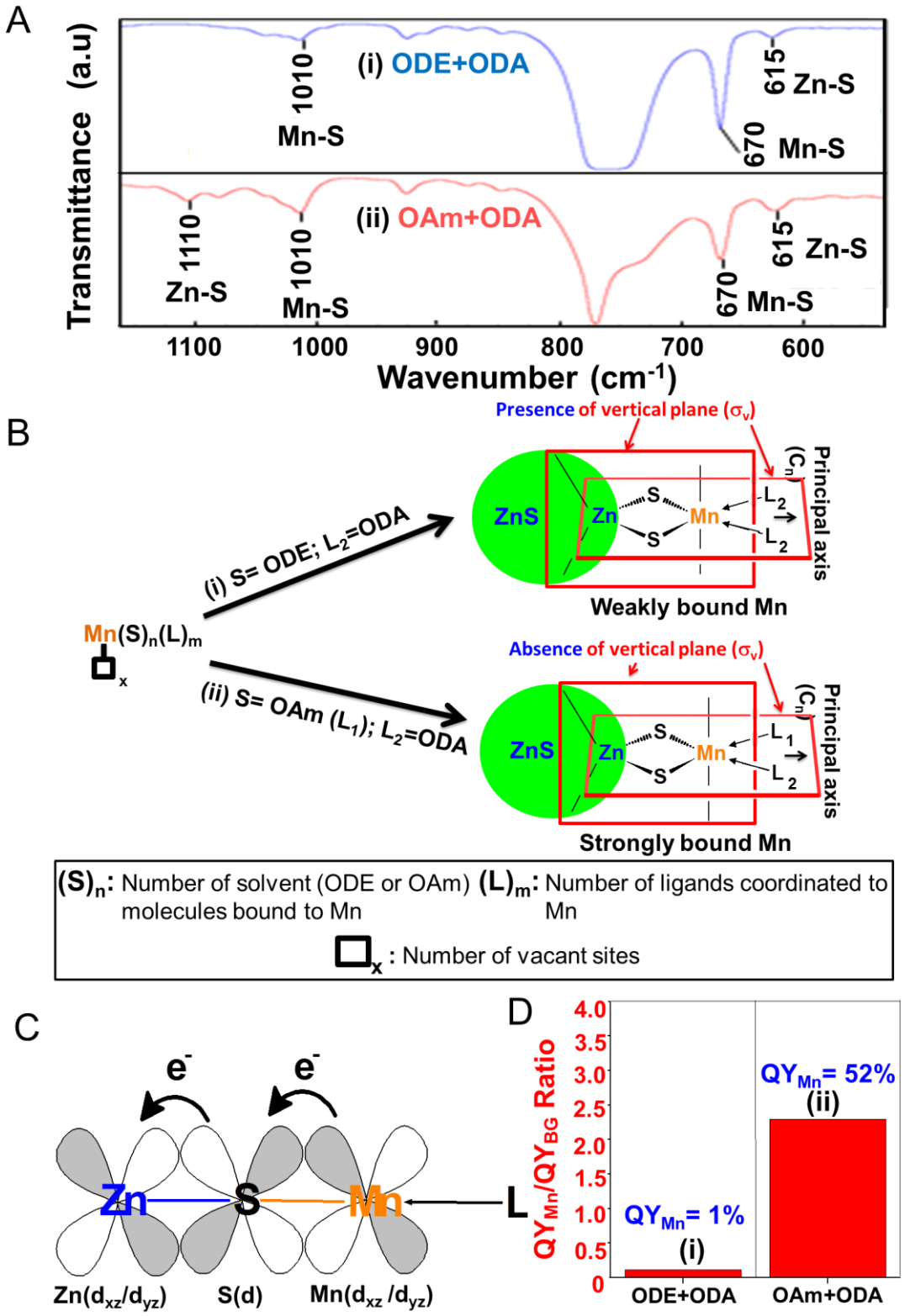

Figure 4. Role of ligands on the binding strength of Mn. (A) FTIR spectra of ZnS:Mn nanocrystals functionalized with (i) [ODE+ODA] and (ii) [OAm+ODA]. (B) Schematic description of the binding strength of Mn to ZnS nanocrystals via two synthetic routes: Mn-complex containing a vacant site coordinates to the sulfur site on the surface of nanocrystals, forming (i) weakly bound Mn and (ii) strongly

bound Mn. The vertical plane (σ_v) denotes the ZnS nanocrystals through the plane containing the principal axis (C_n). (C) Orbital diagram explaining the π back donation through the coordination of ligand (L) to Mn, S and Zn (Zn-S-Mn). (D) The amount of Mn per nanocrystal, represented by quantum yield ratio of Mn and bandgap emissions (QY_{Mn}/QY_{BG}), is given in red for samples (i) and (ii). The corresponding QY_{Mn} is given in blue.

Biological Applications of Doped Nanocrystals. ZnS is a good host for three-photon excitation of doped ZnS nanocrystals. Recently, Hyeon and coworkers[60] have demonstrated the three-photon biomedical imaging application of doped ZnS nanocrystals. First, the role of ligand is to provide a high PLQY in the growth solution through effective surface passivation. Secondly, it is important to retain this high PLQY in aqueous solution, especially for biological applications. We have coated the doped nanocrystals with GSH and finally incorporated them into mesoporous silica nanoparticles. We have chosen GSH (based on our previous experience in imparting good water solubility to CdSe/ZnS quantum dots)[10] to transfer the doped nanocrystals into water. The GSH coating on doped nanocrystals preserved the higher PL-QY (ca. 50%) in water or biological buffers. However, the incorporation of nanocrystals into silica decreased the QY to ca. 35-40%. We believe the retention of QY could be improved further with thin silica coating approach discussed elsewhere[61] for other nanoparticles and quantum dots.

In order to test the applicability of doped ZnS nanocrystals for biological application, we first carried out the cytotoxicity studies on HeLa and CHO cells with different concentrations of GSH-coated ZnS:Mn nanocrystals and found that the cells were healthy with a viability of up to 94-96% at the particle concentration of 0.1 µg/mL (Figure S8). Likewise, ZnS:Mn@GSH@Silica particles exhibited less toxicity on both cell lines at the highest concentration of 0.1 µg/mL. The cell viability at this concentration was close to 88 and 92% for CHO and HeLa cells, respectively (Figures 5A, 5B).

Before performing the labelling of HeLa cells with nanocrystals, we tested the control cells (Figure S8) without treatment of nanocrystal samples under different conditions (transmission DIC image and fluorescence images with RFP and 580 nm filters). We have observed that the untreated cells showed a minimal auto-fluorescence (Figure S9).

Figure 6A-D show the labelling of HeLa cells with ZnS:Mn@GSH@Silica. It is obvious that the cells are healthier after treatment with the nanocrystals, indicating that they are not toxic to single live cell imaging studies and the fluorescence intensity is quite stable to carry out long time imaging studies. Furthermore, it is clear that the nanocrystals are localized mainly in the perinuclear region (labelling around the nucleus) of the cells, which implies that the cells can carry out normal biological functions in

the presence of nanocrystals. The localization of coated nanocrystals at the perinuclear region is in consonance with our earlier work on ZnS:Cu doped nanocrystals.[38]

Figure 7A compares the encapsulation efficiency of anticancer drug, doxorubicin (DOX) into silica nanoparticles prepared by the coating of ZnS:Mn nanocrystals with either silica alone or a dual coating method by GSH/mesoporous silica. At a given drug loading concentration (50-300 µg), GSH coated nanocrystals (ZnS:Mn@GSH@Silica) increased the encapsulation efficiency of DOX up to 90-95% in comparison with silica coated nanocrystals (ZnS:Mn@Silica), where the encapsulation efficiency of DOX decreased from ca. 88% to 40% at higher drug loading. Figure 7B shows the in-vitro cumulative release profile of DOX over a period of 72 h at two different pH values. At pH 7.4 the release was much slower (< 20%) even after 72 h whereas the release was faster at pH 5.3. Most of the drug (> 90%) was released within the first 10 h at the ideal pH of 5.3 for cancer cells.

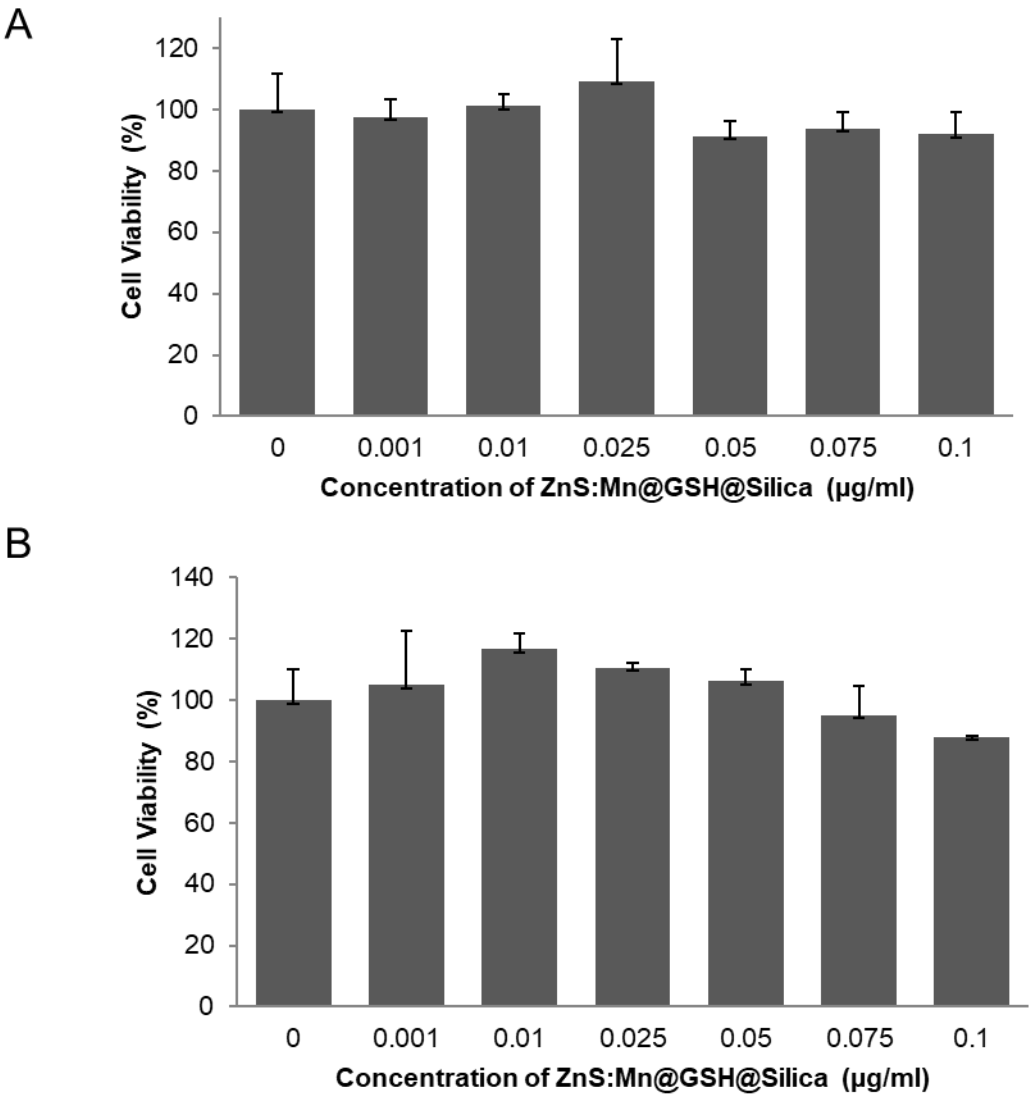

Figure 5. Cell viability of (A) HeLa and (B) CHO cells after 24 h of incubation with ZnS:Mn@GSH@Silica nanocrystals.

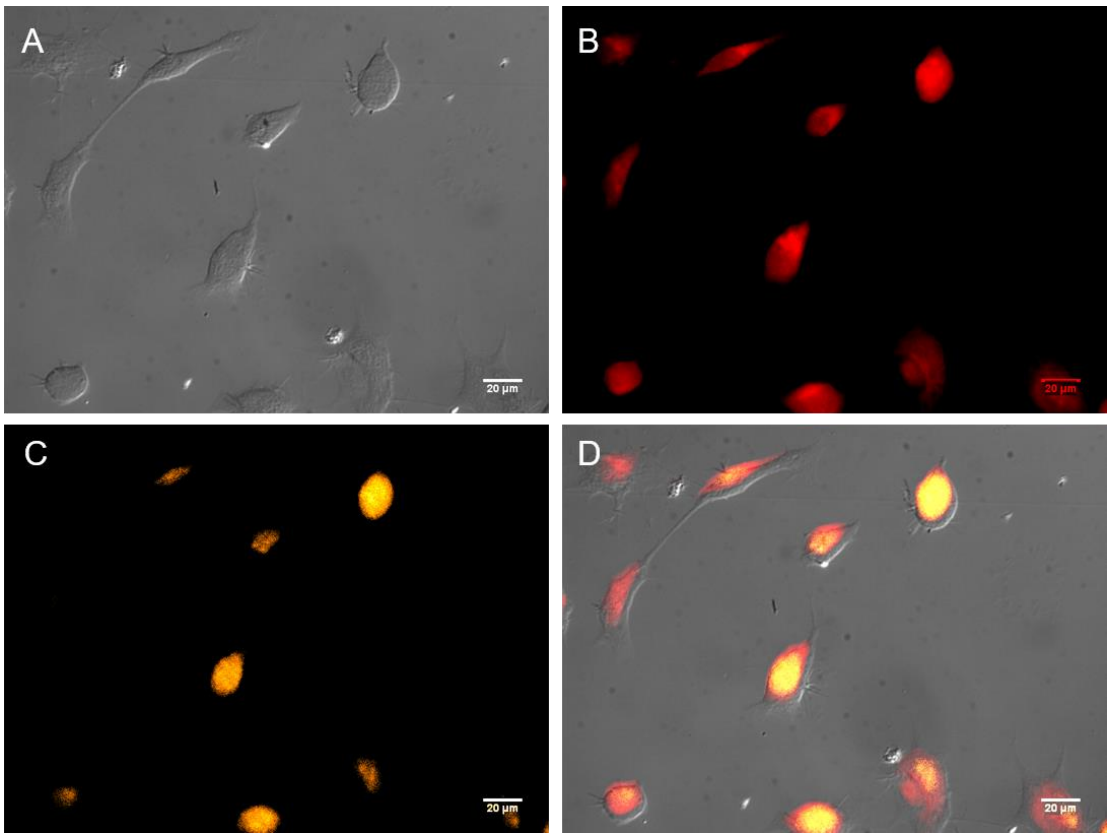

Figure 6. Labelling of HeLa cells with doped nanocrystals. (A) Transmission image in DIC channel, (B) fluorescence under RFP filter (C) fluorescence under 580 nm filter and (D) overlaid image of HeLa cells labelled with ZnS:Mn@GSH@Silica. Scale bar: 20 µm.

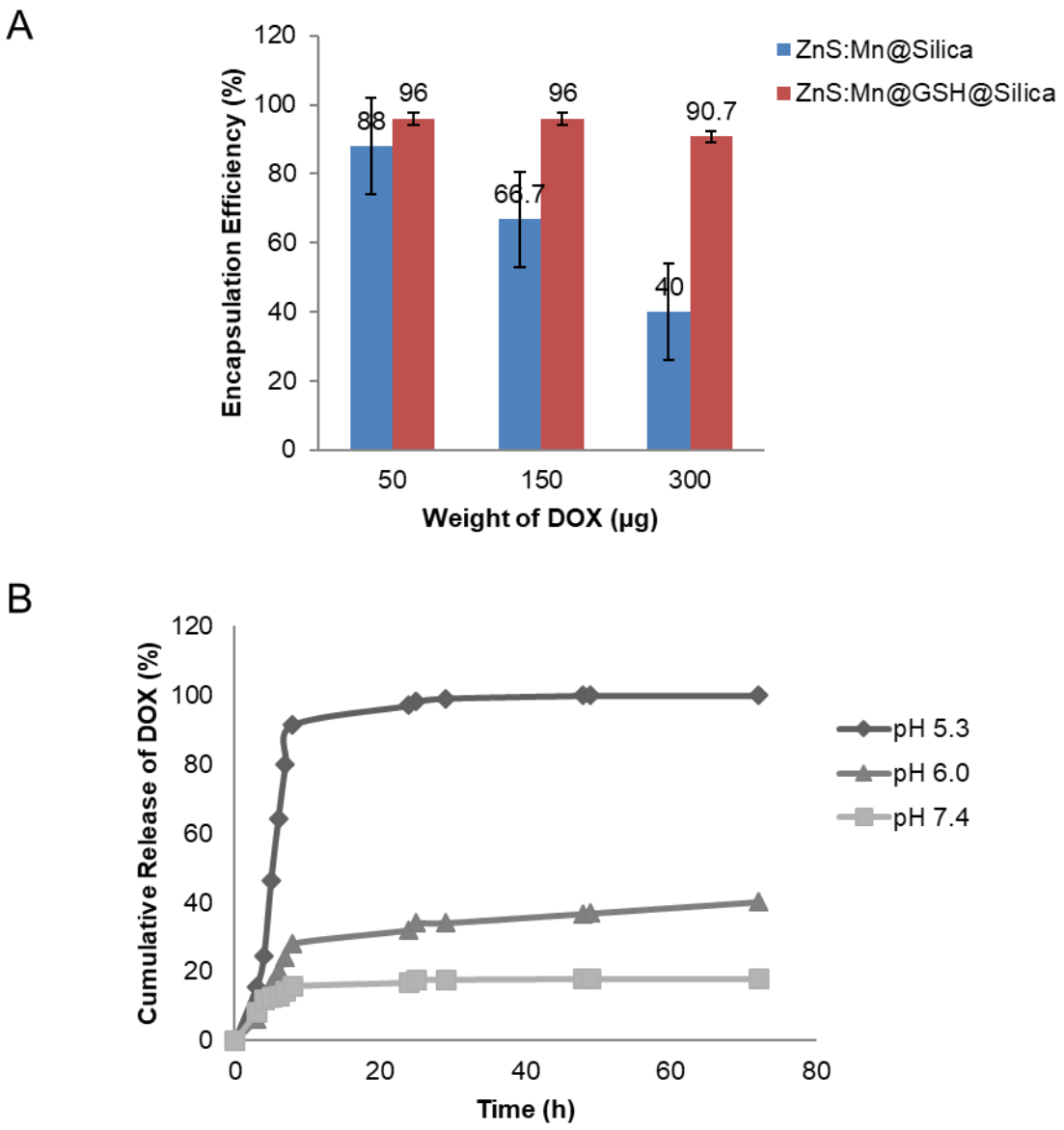

Figure 7. Doped nanocrystals for drug delivery. (A) The encapsulation efficiency of anticancer drug, doxorubicin (DOX) in silica nanoparticles at different drug loading concentration: (i) ZnS:Mn@Silica and (ii) ZnS:Mn@GSH@Silica. (B) Effect of pH on the release profile of DOX over a period of 72 h for ZnS:Mn@GSH@Silica.

4. CONCLUSION

In conclusion, we have demonstrated a dual ligand (OAm and ODA) method for the synthesis of organic-soluble ZnS:Mn nanocrystals (QY: ~80%). This study has unravelled the effects of ligand base strength and dopant–ligand complex on the formation of highly fluorescent nanocrystals. We have also

shown the transfer of organic-soluble doped ZnS:Mn nanocrystals into water-soluble nanocrystals by means of either GSH and (GSH and silica) coating method with the retention of a considerable QY of ~50% and 35%, respectively. Furthermore, the in vitro bio-labelling and drug release studies have demonstrated clearly the potential applications of doped ZnS:Mn nanocrystals. We believe this work will bring new insights into this emerging area of doped nanocrystals.

ASSOCIATED CONTENT

Supporting Information

Fluorescent digital images of both GSH and silica-coated nanocrystals; HRTEM images with FFT, time resolved emission spectra, XRD patterns, and FTIR spectra for as-synthesized ZnS:Mn nanocrystals with different dual ligands; cell viability of HeLa and CHO cells with ZnS:Mn@GSH nanocrystals; transmission (DIC) and fluorescence images of control HeLa cells without treatment of doped nanocrystals.

The Supporting Information is available free of charge on the ACS Publications website at DOI:

Corresponding Authors

*(E.H.A.) E-mail: edison.ang@nie.edu.sg

*(S.T.S.) E-mail: subra.selvan@ntu.edu.sg

ORCID

Edison Ang Huixiang: 0000-0002-7869-268X

Subramanian Tamil Selvan: 0000-0002-1524-2374

Notes

The authors declare no competing financial interest.

ACKNOWLEDGMENTS

We acknowledge funding from the Joint Council Office, A*STAR, Singapore (Grant No. JCOAG03-FG03). We thank the core facilities (XRD, TEM) support staff at the Institute of Materials Research and Engineering (IMRE, Singapore). H.A. and S.T.S. acknowledge the National Institution of Education (NIE) and LKC School of Medicine NTU, respectively, for their support in completing and publishing this work.

REFERENCES

1. Fan, W.; Yung, B.; Huang, P.; Chen, X., Nanotechnology for multimodal synergistic cancer therapy. *Chemical reviews* **2017,** *117* (22), 13566-13638.
2. Nanda, S. S.; Hembram, K.; Lee, J.-K.; Kim, K.; Selvan, S. T.; Yi, D. K., Experimental and Theoretical Structural Characterization of Cu–Au Tripods for Photothermal Anticancer Therapy. *ACS Applied Nano Materials* **2019,** *2* (6), 3735-3742.
3. Wicki, A.; Witzigmann, D.; Balasubramanian, V.; Huwyler, J., Nanomedicine in cancer therapy: challenges, opportunities, and clinical applications. *Journal of controlled release* **2015,** *200*, 138-157.
4. Selvan, S.T.; Padmanabhan, P.; Gulyás, B.Z., Nanotechnology-Based Diagnostics and Therapy for Pathogen-Related Infections in the CNS. *ACS Chemical Neuroscience* **2019**, https://doi.org/10.1021/acschemneuro.9b00470.
5. Ramanathan, S.; Archunan, G.; Sivakumar, M.; Selvan, S. T.; Fred, A. L.; Kumar, S.; Gulyás, B.; Padmanabhan, P., Theranostic applications of nanoparticles in neurodegenerative disorders. *International journal of nanomedicine* **2018,** *13*, 5561.
6. Pradhan, N.; Jana, N. R.; Jana, N. R., Inhibition of protein aggregation by iron oxide nanoparticles conjugated with glutamine-and proline-based osmolytes. *ACS Applied Nano Materials* **2018,** *1* (3), 1094-1103.
7. Debnath, K.; Jana, N. R.; Jana, N. R., Designed Polymer Micelle for Clearing Amyloid Protein Aggregates via Up-Regulated Autophagy. *ACS Biomaterials Science & Engineering* **2018,** *5* (1), 390-401.
8. Medintz, I. L.; Mattoussi, H.; Clapp, A. R., Potential clinical applications of quantum dots. *International journal of nanomedicine* **2008,** *3* (2), 151.
9. Selvan, S. T., Silica-coated quantum dots and magnetic nanoparticles for bioimaging applications (Mini-Review). *Biointerphases* **2010,** *5* (3), FA110-FA115.
10. Narayanan, K.; Yen, S. K.; Dou, Q.; Padmanabhan, P.; Sudhaharan, T.; Ahmed, S.; Ying, J. Y.; Selvan, S. T., Mimicking cellular transport mechanism in stem cells through endosomal escape of new peptide-coated quantum dots. *Scientific reports* **2013,** *3*, 2184.
11. Fu, Y.-S.; Du, X.-W.; Kulinich, S. A.; Qiu, J.-S.; Qin, W.-J.; Li, R.; Sun, J.; Liu, J., Stable aqueous dispersion of ZnO quantum dots with strong blue emission via simple solution route. *Journal of the American Chemical Society* **2007,** *129* (51), 16029-16033.
12. Hong, G.; Robinson, J. T.; Zhang, Y.; Diao, S.; Antaris, A. L.; Wang, Q.; Dai, H., In vivo fluorescence imaging with Ag2S quantum dots in the second near-infrared region. *Angewandte Chemie International Edition* **2012,** *51* (39), 9818-9821.
13. Chen, G.; Tian, F.; Zhang, Y.; Zhang, Y.; Li, C.; Wang, Q., Tracking of transplanted human mesenchymal stem cells in living mice using near-infrared Ag2S quantum dots. *Advanced Functional Materials* **2014,** *24* (17), 2481-2488.
14. Chen, H.; Li, B.; Zhang, M.; Sun, K.; Wang, Y.; Peng, K.; Ao, M.; Guo, Y.; Gu, Y., Characterization of tumor-targeting Ag 2 S quantum dots for cancer imaging and therapy in vivo. *Nanoscale* **2014,** *6* (21), 12580-12590.
15. Ochsenbein, S. T.; Feng, Y.; Whitaker, K. M.; Badaeva, E.; Liu, W. K.; Li, X.; Gamelin, D. R., Charge-controlled magnetism in colloidal doped semiconductor nanocrystals. *Nature nanotechnology* **2009,** *4* (10), 681.
16. Pandey, A.; Brovelli, S.; Viswanatha, R.; Li, L.; Pietryga, J.; Klimov, V. I.; Crooker, S., Long-lived photoinduced magnetization in copper-doped ZnSe–CdSe core–shell nanocrystals. *Nature nanotechnology* **2012,** *7* (12), 792.

17. Norris, D. J.; Efros, A. L.; Erwin, S. C., Doped nanocrystals. *Science* **2008,** *319* (5871), 1776-1779.
18. Wu, P.; Yan, X.-P., Doped quantum dots for chemo/biosensing and bioimaging. *Chemical Society Reviews* **2013,** *42* (12), 5489-5521.
19. Pradhan, N.; Battaglia, D. M.; Liu, Y.; Peng, X., Efficient, stable, small, and water-soluble doped ZnSe nanocrystal emitters as non-cadmium biomedical labels. *Nano Letters* **2007,** *7* (2), 312-317.
20. Ehlert, O.; Bücking, W.; Riegler, J.; Merkulov, A.; Nann, T., Organometallic synthesis and electrophoretic characterization of high-quality ZnS: Mn/ZnS core/shell nanoparticles for bioanalytical applications. *Microchimica Acta* **2008,** *160* (3), 351-356.
21. Erwin, S. C.; Zu, L.; Haftel, M. I.; Efros, A. L.; Kennedy, T. A.; Norris, D. J., Doping semiconductor nanocrystals. *Nature* **2005,** *436* (7047), 91.
22. Ehlert, O.; Osvet, A.; Batentschuk, M.; Winnacker, A.; Nann, T., Synthesis and spectroscopic investigations of Cu-and Pb-doped colloidal ZnS nanocrystals. *The Journal of Physical Chemistry B* **2006,** *110* (46), 23175-23178.
23. Bhargava, R.; Gallagher, D.; Hong, X.; Nurmikko, A., Optical properties of manganese-doped nanocrystals of ZnS. *Physical Review Letters* **1994,** *72* (3), 416.
24. Deng, Z.; Tong, L.; Flores, M.; Lin, S.; Cheng, J.-X.; Yan, H.; Liu, Y., High-quality manganese-doped zinc sulfide quantum rods with tunable dual-color and multiphoton emissions. *Journal of the American Chemical Society* **2011,** *133* (14), 5389-5396.
25. Karan, N. S.; Sarma, D.; Kadam, R.; Pradhan, N., Doping transition metal (Mn or Cu) ions in semiconductor nanocrystals. *The Journal of Physical Chemistry Letters* **2010,** *1* (19), 2863-2866.
26. Sarkar, S.; Patra, B. K.; Guria, A. K.; Pradhan, N., The redox chemistry at the interface for retrieving and brightening the emission of doped semiconductor nanocrystals. *The journal of physical chemistry letters* **2013,** *4* (12), 2084-2090.
27. Acharya, S.; Sarkar, S.; Pradhan, N., Material diffusion and doping of Mn in wurtzite ZnSe nanorods. *The Journal of Physical Chemistry C* **2013,** *117* (11), 6006-6012.
28. Pradhan, N.; Sarma, D., Advances in light-emitting doped semiconductor nanocrystals. *The Journal of Physical Chemistry Letters* **2011,** *2* (21), 2818-2826.
29. Nag, A.; Chakraborty, S.; Sarma, D., To dope Mn2+ in a semiconducting nanocrystal. *Journal of the American Chemical Society* **2008,** *130* (32), 10605-10611.
30. Pradhan, N.; Goorskey, D.; Thessing, J.; Peng, X., An alternative of CdSe nanocrystal emitters: pure and tunable impurity emissions in ZnSe nanocrystals. *Journal of the American Chemical Society* **2005,** *127* (50), 17586-17587.
31. Pradhan, N.; Peng, X., Efficient and color-tunable Mn-doped ZnSe nanocrystal emitters: control of optical performance via greener synthetic chemistry. *Journal of the American Chemical Society* **2007,** *129* (11), 3339-3347.
32. Srivastava, B. B.; Jana, S.; Karan, N. S.; Paria, S.; Jana, N. R.; Sarma, D.; Pradhan, N., Highly luminescent Mn-doped ZnS nanocrystals: gram-scale synthesis. *The Journal of Physical Chemistry Letters* **2010,** *1* (9), 1454-1458.
33. Zu, L.; Norris, D. J.; Kennedy, T. A.; Erwin, S. C.; Efros, A. L., Impact of ripening on manganese-doped ZnSe nanocrystals. *Nano letters* **2006,** *6* (2), 334-340.
34. Yang, Y.; Chen, O.; Angerhofer, A.; Cao, Y. C., On doping CdS/ZnS core/shell nanocrystals with Mn. *Journal of the American Chemical Society* **2008,** *130* (46), 15649-15661.
35. Norris, D. J.; Yao, N.; Charnock, F. T.; Kennedy, T. A., High-quality manganese-doped ZnSe nanocrystals. *Nano Letters* **2001,** *1* (1), 3-7.
36. Du, M.-H.; Erwin, S. C.; Efros, A. L., Trapped-dopant model of doping in semiconductor nanocrystals. *Nano letters* **2008,** *8* (9), 2878-2882.
37. Yang, Y.; Chen, O.; Angerhofer, A.; Cao, Y. C., Radial-position-controlled doping of CdS/ZnS core/shell nanocrystals: surface effects and position-dependent properties. *Chemistry–A European Journal* **2009,** *15* (13), 3186-3197.

38. Ang, H.; Bosman, M.; Thamankar, R.; Zulkifli, M. F. B.; Yen, S. K.; Hariharan, A.; Sudhaharan, T.; Selvan, S. T., Highly Luminescent Heterostructured Copper-Doped Zinc Sulfide Nanocrystals for Application in Cancer Cell Labeling. *ChemPhysChem* **2016,** *17* (16), 2489-2495.
39. Dinda, S.; Kakran, M.; Zeng, J.; Sudhaharan, T.; Ahmed, S.; Das, D.; Selvan, S. T., Grafting of ZnS: Mn-Doped Nanocrystals and an Anticancer Drug onto Graphene Oxide for Delivery and Cell Labeling. *ChemPlusChem* **2016,** *81* (1), 100-107.
40. Sung, Y.-M.; Gayam, S. R.; Hsieh, P.-Y.; Hsu, H.-Y.; Diau, E. W.-G.; Wu, S.-P., Quinone-modified Mn-doped ZnS quantum dots for room-temperature phosphorescence sensing of human cancer cells that overexpress NQO1. *ACS applied materials & interfaces* **2015,** *7* (46), 25961-25969.
41. Selvan, S. T.; Tan, T. T.; Ying, J. Y., Robust, non-cytotoxic, silica-coated CdSe quantum dots with efficient photoluminescence. *Advanced Materials* **2005,** *17* (13), 1620-1625.
42. Yi, D. K.; Selvan, S. T.; Lee, S. S.; Papaefthymiou, G. C.; Kundaliya, D.; Ying, J. Y., Silica-coated nanocomposites of magnetic nanoparticles and quantum dots. *Journal of the American Chemical Society* **2005,** *127* (14), 4990-4991.
43. Tan, T. T.; Selvan, S. T.; Zhao, L.; Gao, S.; Ying, J. Y., Size control, shape evolution, and silica coating of near-infrared-emitting PbSe quantum dots. *Chemistry of Materials* **2007,** *19* (13), 3112-3117.
44. Selvan, S. T.; Li, C.; Ando, M.; Murase, N., Formation of luminescent CdTe–Silica nanoparticles through an inverse microemulsion technique. *Chemistry letters* **2004,** *33* (4), 434-435.
45. Gerion, D.; Pinaud, F.; Williams, S. C.; Parak, W. J.; Zanchet, D.; Weiss, S.; Alivisatos, A. P., Synthesis and properties of biocompatible water-soluble silica-coated CdSe/ZnS semiconductor quantum dots. *The Journal of Physical Chemistry B* **2001,** *105* (37), 8861-8871.
46. Mulvaney, P.; Liz-Marzan, L.; Giersig, M.; Ung, T., Silica encapsulation of quantum dots and metal clusters. *Journal of Materials Chemistry* **2000,** *10* (6), 1259-1270.
47. Zhelev, Z.; Ohba, H.; Bakalova, R., Single quantum dot-micelles coated with silica shell as potentially non-cytotoxic fluorescent cell tracers. *Journal of the American Chemical Society* **2006,** *128* (19), 6324-6325.
48. Darbandi, M.; Thomann, R.; Nann, T., Single quantum dots in silica spheres by microemulsion synthesis. *Chemistry of materials* **2005,** *17* (23), 5720-5725.
49. Selvan, S. T.; Patra, P. K.; Ang, C. Y.; Ying, J. Y., Synthesis of silica-coated semiconductor and magnetic quantum dots and their use in the imaging of live cells. *Angewandte Chemie International Edition* **2007,** *46* (14), 2448-2452.
50. Palui, G.; Aldeek, F.; Wang, W.; Mattoussi, H., Strategies for interfacing inorganic nanocrystals with biological systems based on polymer-coating. *Chemical Society Reviews* **2015,** *44* (1), 193-227.
51. Yen, S. K.; Janczewski, D.; Lakshmi, J. L.; Dolmanan, S. B.; Tripathy, S.; Ho, V. H.; Vijayaragavan, V.; Hariharan, A.; Padmanabhan, P.; Bhakoo, K. K., Design and synthesis of polymer-functionalized NIR fluorescent dyes–magnetic nanoparticles for bioimaging. *ACS nano* **2013,** *7* (8), 6796-6805.
52. Topete, A.; Alatorre-Meda, M.; Villar-Alvarez, E. M.; Carregal-Romero, S.; Barbosa, S.; Parak, W. J.; Taboada, P.; Mosquera, V., Polymeric-Gold Nanohybrids for Combined Imaging and Cancer Therapy. *Advanced healthcare materials* **2014,** *3* (8), 1309-1325.
53. Zhang, P.; Cui, Y.; Anderson, C. F.; Zhang, C.; Li, Y.; Wang, R.; Cui, H., Peptide-based nanoprobes for molecular imaging and disease diagnostics. *Chemical Society Reviews* **2018,** *47* (10), 3490-3529.
54. Weng, K. C.; Noble, C. O.; Papahadjopoulos-Sternberg, B.; Chen, F. F.; Drummond, D. C.; Kirpotin, D. B.; Wang, D.; Hom, Y. K.; Hann, B.; Park, J. W., Targeted tumor cell internalization and imaging of multifunctional quantum dot-conjugated immunoliposomes in vitro and in vivo. *Nano letters* **2008,** *8* (9), 2851-2857.
55. Al-Jamal, W. T.; Al-Jamal, K. T.; Tian, B.; Cakebread, A.; Halket, J. M.; Kostarelos, K., Tumor targeting of functionalized quantum dot− liposome hybrids by intravenous administration. *Molecular pharmaceutics* **2009,** *6* (2), 520-530.

56. Scaletti, F.; Hardie, J.; Lee, Y.-W.; Luther, D. C.; Ray, M.; Rotello, V. M., Protein delivery into cells using inorganic nanoparticle–protein supramolecular assemblies. *Chemical Society Reviews* **2018,** *47* (10), 3421-3432.
57. Chithrani, B. D.; Chan, W. C., Elucidating the mechanism of cellular uptake and removal of protein-coated gold nanoparticles of different sizes and shapes. *Nano letters* **2007,** *7* (6), 1542-1550.
58. Fischer, S. A.; Crotty, A. M.; Kilina, S. V.; Ivanov, S. A.; Tretiak, S., Passivating ligand and solvent contributions to the electronic properties of semiconductor nanocrystals. *Nanoscale* **2012,** *4* (3), 904-914.
59. Norman, T. J.; Magana, D.; Wilson, T.; Burns, C.; Zhang, J. Z.; Cao, D.; Bridges, F., Optical and surface structural properties of Mn2+-doped ZnSe nanoparticles. *The Journal of Physical Chemistry B* **2003,** *107* (26), 6309-6317.
60. Yu, J. H.; Kwon, S.-H.; Petrášek, Z.; Park, O. K.; Jun, S. W.; Shin, K.; Choi, M.; Park, Y. I.; Park, K.; Na, H. B., High-resolution three-photon biomedical imaging using doped ZnS nanocrystals. *Nature materials* **2013,** *12* (4), 359.
61. Jana, N. R.; Earhart, C.; Ying, J. Y., Synthesis of water-soluble and functionalized nanoparticles by silica coating. *Chemistry of Materials* **2007,** *19* (21), 5074-5082.